An implicit wetting–drying algorithm for the discontinuous Galerkin method
Application to the Tonle Sap, Mekong River Basin

Le, Hoang Anh; Lambrechts, Jonathan; Ortleb, Sigrun; Gratiot, Nicolas; Deleersnijder, Eric; Soares-Frazão, Sandra

DOI
10.1007/s10652-019-09732-7

Publication date
2020

Document Version
Accepted author manuscript

Published in
Environmental Fluid Mechanics

Citation (APA)
Le, H. A., Lambrechts, J., Ortleb, S., Gratiot, N., Deleersnijder, E., & Soares-Frazão, S. (2020). An implicit wetting–drying algorithm for the discontinuous Galerkin method: Application to the Tonle Sap, Mekong River Basin. *Environmental Fluid Mechanics*, *20*(4), 923-951. https://doi.org/10.1007/s10652-019-09732-7

Published in "Environmental Fluid Mechanics"
doi:10.1007/s10652-019-09732-7

Noname manuscript No.
(will be inserted by the editor)

An implicit wetting - drying algorithm for the Discontinuous Galerkin method: Application to the Tonle Sap, Mekong River Basin

Hoang-Anh Le · Jonathan Lambrechts · Sigrun Ortleb · Nicolas Gratiot · Eric Deleersnijder · Sandra Soares-Frazão

Received: date / Accepted: date

Abstract The accurate simulation of wetting - drying processes in floodplains and coastal zones is a challenge for hydrodynamic modelling, especially for long time simulations. Indeed, dedicated numerical procedures are generally time-consuming, instabilities can occur at the wet/dry front, rapid transition of wet/dry interface and mass conservation are not always ensured. We present the extension of an existing wetting - drying algorithm in two space dimensions and its application to a real case. The wetting - drying algorithm is implemented in SLIM (Second-generation Louvain-la-Neuve Ice-ocean Model, www.slim-ocean.be), a discontinuous Galerkin finite element model (DG-FEM) solving the shallow water equations in a fully implicit way. This algorithm consists in applying a threshold value of

Hoang-Anh Le · Jonathan Lambrechts · Eric Deleersnijder · Sandra Soares-Frazão
Institute of Mechanics, Materials and Civil Engineering (IMMC), Université catholique de Louvain, Place du Levant 1, B-1348 Louvain-la-Neuve, Belgium
Tel.: + 32 (0)10 47 21 25
Fax: + 32 (0)10 47 21 79

Hoang-Anh Le · Nicolas Gratiot
Asian Research Center on Water (CARE-Rescif), Ho Chi Minh City University of Technology, Block B7, 268 Ly Thuong Kiet Street, District 10, Ho Chi Minh City, Vietnam
Tel.: +84 (28) 38 647 256
Fax: +84 (28) 38 653 823

Sigrun Ortleb
Universität Kassel, FB 10, Institut für Mathematik, Heinrich-Plett-Straße 40, D-34132 Kassel, Germany

Nicolas Gratiot
Université Grenoble Alpes, CNRS, IRD, Grenoble INP, IGE, F-38000 Grenoble, France

Eric Deleersnijder
Earth and Life Institute (ELI), Université catholique de Louvain, Avenue Georges Lemaître 4, B-1348 Louvain-la-Neuve, Belgium
Delft University of Technology, Delft Institute of Applied Mathematics (DIAM), Van Mourik Broekmanweg 6, 2628XE Delft, The Netherlands

E-mail: anh.le@uclouvain.be

fluid depth for a thin layer and a blending parameter in order to guarantee positive values of the water depth, while preserving local mass conservation and the well balanced property at wet/dry interfaces. The technique is first validated against standard analytical test cases (Balzano 1, Balzano 3 and Thacker test cases) and is subsquently applied in a realistic domain, the Tonle Sap Lake in the Mekong River Basin, where the water level can vary by about 10 m between the dry and the wet season.

Keywords numerical model · wetting - drying · SLIM · DG-FEM · Mekong · Tonle Sap lake

1 Introduction

Floodplains have indisputable roles in river basins over the world [1] by providing livelihood for riparian residents [2], biodiversity of river ecosystems [3] as well as reducing flood risks for the downstream areas [4]. However, floodplains are subject to river floods or flow regulation inducing possible long periods of inundation with wetting and drying phases [5]. These phenomena impact both the physical and biological aspects of the domain [6], especially during extreme events such as tsunamis and storm surges [7], affecting the natural functions of floodplains. Thus, an accurate representation of wetting - drying processes in a floodplain, and adjacent continental water bodies, is a crucial issue for hydrodynamic models. Dealing with very shallow flows, temporary submergences, a wide spectrum of time scales and complex morphologies, high spatial and temporal resolutions often require [8] large computational time. Even with the development of powerful and parallel computers (e.g. [9]), the question of computational time remains an open challenge for geoscience modellers addressing large domains and long-lasting floods.

Wetting - drying is an issue that has received considerable attention since decades [10]. In early developments, the prevailing strategy of most hydraulic modellers was to adopt mesh deformation at the wet/dry front. However, it was recognized that this approach was quite difficult in the context of complex bathymetries and flow configurations [9, 11, 10, 7] because the nodal coordinates vary at each time step and parameterization is required for moving the boundaries according to the flow variables. Recent research focuses on developing wetting - drying algorithms for fixed meshes. All schemes must satisfy both local and global mass conservation together with momentum conservation [12]. According to [8], four categories of wetting - drying algorithms can be considered:

(1) Element removal algorithm: elements are considered as being dry or wet, and dry elements are removed from the computational domain. The drawback of this procedure is that mass and momentum conservation may be broken, possibly causing the numerical simulation to be unstable [10].

(2) Thin layer: a threshold depth is imposed in the whole computational domain, ensuring positive water depths. If the water depth falls below this threshold in a given element, this element is considered dry and the corresponding velocity is set to zero. This threshold depth, however, corresponds to a substantial water volume in the dry areas [13], leading to possible mass conservation issues. However, the strongest advantage of this approach is that it is easily applicable in two- or three-

dimensions (2D or 3D) [11]. The drawback of this algorithm is a rapid transfer of elements from dry to wet states near the wetting front that increases the stiffness of the problem, restricting the time step in explicit temporal discretisation and worsening the conditioning of the non-linear system in implicit temporal discretisation. The algorithm also requires a higher spatial mesh resolution, resulting therefore in increased computational time.
(3) Depth extrapolation algorithms: a new depth in the dry cells is extrapolated from the surrounding wet cells. The modified depth is then used to compute the velocity. The concerned cells are thus integrated into the wet domain. However, this artificial wetting of dry elements causes artificial leakage between adjacent cells [14]. Mass conservation is affected and, hence, needs to be enforced by corrective schemes [15].
(4) Negative depth algorithms or so-called artificial porosity approach: the model can run with negative depths, the subsurface flow being controlled by porosity terms. The advantage of this method is that it is no longer required to separate wet and dry cells [11] and a smooth transition between wet and dry cells is ensured [10]. However, the method has several disadvantages. As the artificial porosity is applied not only to negative depths but also to a certain height above the actual sea bottom or riverbed [16], it results in unphysical properties in the fictitious porous layers. In addition, a lack of mass conservation is observed [11] because of artificial mass transfers from dry to wet areas [17].
Even though semi-implicit schemes exist [10], most of the current methods resort to explicit time-marching schemes, which are constrained by the Courant-Friedrichs-Lewy (CFL) condition [18–20]. Explicit time integration requires high temporal resolutions making such schemes rather expensive in terms of computational cost. Therefore they are not suitable for large-scale and complex domains and for long time simulations.
The present work is an attempt to overcome the weaknesses mentioned above by implementing the implicit algorithm developed by [7] in SLIM (Second-generation Louvain-la-Neuve Ice-ocean Model, www.slim-ocean.be), a discontinuous Galerkin finite element model (DG-FEM) with an open source code. The algorithm is first tested against several cases with analytical solutions before being applied in a natural domain. The aim is to simulate the flow in Lake Tonle Sap, an integral part of the Mekong River system. In this system, the variation of the water depth can reach 10 m and the inundation area can increase nearly nine folds from dry season to wet season; the bottom is rather rugged with many narrow tributaries. It also experiences a reverse flow direction from wet to dry season. So a complex domain has never been tacked by means of SLIM. The various flow regimes must be dealt by an algorithm that is computationally efficient, ensures mass conservation and provides a suitable treatment of wet/dry interfaces.
Accordingly, this paper is organized as follows: first, the implicit wetting - drying algorithm as implemented in SLIM is presented; then the validation test cases with analytical solutions are run, and lastly the application to the Tonle Sap system is presented, during a flooding year and a dry year. Finally, conclusions about the performance of the proposed scheme are drawn.

2 Wetting - drying scheme

2.1 The SLIM finite element model

SLIM is a hydrodynamic model based on DG-FEM over unstructured grids that has been developed at the Université catholique de Louvain, Belgium for more than ten years. SLIM includes different options, ranging from one- to three-dimensional (1D to 3D) modules: the 1D version is a section-averaged model for river networks; the 2D depth-averaged version is generally applied to shallow, complex domains; the 3D version is a baroclinic model for coastal flows that solves the 3D hydrostatic equations under the Boussinesq approximation; there are two additional modules (Lagrangian particle tracker and Eulerian transport model). This approach provides an adequate degree of flexibility both geometrically and functionally as it can accurately represent complex topographies and also model solutions with sharp gradients. Unlike more standard numerical methods, such as finite volumes, it introduces a minimal amount of numerical dissipation and thus preserves small-scale flow features such as recirculation eddies.
The model has been applied to various domains such as Lake Tanganyika, Africa [21], the Great Barrier Reef, Australia [22], the Scheldt estuary, Belgium and Netherlands [23], the Mahakam Delta, Indonesia [24, 25], the Columbia River, USA [26], and various lakes of Titan, Saturn's moon [27]. Flow field, sediment transport, water renewal time scales and ecological issues were tackled.

2.2 Governing equations

The shallow-water equations are derived by integrating over the water column the Navier-Stokes equations, assuming that the pressure is hydrostatic and the fluid density is constant. Water flows are generally well represented by those equations if the water column is well mixed and the vertical dimension is much smaller than the typical horizontal scale. The conservative shallow water equations read:

$$\frac{\partial H}{\partial t} + \nabla.(H\mathbf{u}) = 0 \tag{1}$$

$$\frac{\partial H\mathbf{u}}{\partial t}+\nabla.\frac{H\mathbf{u}H\mathbf{u}}{H}+g\nabla\frac{|H|H}{2}+\frac{n^2 g}{H^{\frac{7}{3}}}|H\mathbf{u}|H\mathbf{u}+f\mathbf{e}_z\times H\mathbf{u}-\nabla.(H\upsilon\nabla\mathbf{u}) = gH\nabla h \tag{2}$$

where t is time and ∇ is the horizontal del operator; H is the actual water depth, and $\mathbf{u}$ = *(u,v)* is the horizontal velocity vector averaged over the water column; H and $\mathbf{u}$ are the state variables that depend on time and position; η is the free surface elevation, $\eta = H$ - h, where h is the water depth measured from a reference level; f is the Coriolis parameter; $\mathbf{e}_z$ is a vertical unit vector pointing upward; g is the gravitational acceleration ($g = 9.81$ m/s^2); υ is the horizontal eddy viscosity. The latter is parameterized by [28]. The bed shear stress is evaluated with the help of the Chézy - Manning - Strickler formulation with n being the Manning coefficient. These parameters have been calibrated in SLIM for various domains of interest over the world [10, 11, 22–27]. Using a spatially variable Manning coefficient could probably improve the quality of simulations. However, relevent data must be available, especially about the nature of the bottom of the water column.

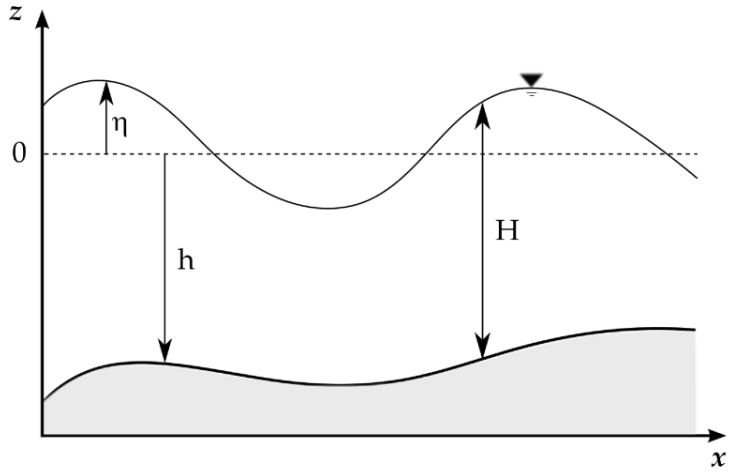

Fig. 1 Water column geometry, where η and h denote the free surface elevation (positive upwards) and the reference depth, respectively. The actual depth of the water column is $H = h + \eta$ [25]

For solving the shallow-water equations, explicit time marching schemes must meet the CFL condition to ensure numerical stability, leading to small values of the time step. Implicit time marching allows for much longer time steps, which is appropriate for meshes with variable resolution and long simulations [18,19], and corresponds to the choice made for the present simulations. To maintain this implicit time stepping efficient even at wet/dry fronts, appropriate algorithms have to be developed. An extension of the 1D algorithm [7] is presented hereinafter.

2.3 Wetting - drying algorithm

The algorithm for an explicit temporal discretisation is detailed in [7]. We focus on its extension to an implicit time scheme because at present, it is the only one able to deal with thin water layers in a DG framework.
Three main problems occur when the water depth becomes zero ($H = 0$): (1) the occurrence of artificial gradients in the surface elevation that can influence the momentum equation and result in an unbalanced scheme; (2) the occurrence of negative depths; (3) ill-conditioned computation of the velocity.
When one node is dry on an element, the DG discretization does not represent the physical situation accurately near the wet/dry interface: two distinct situations can be identified (see Fig. 2(a) and Fig 2(b)). In situation (a), the artifical gradient of surface elevation would remove water from an already dry node. To prevent this, the gravitational force should be ignored on the element. In situation (b), the surface elevation gradient is different from zero and the water flows from higher elevation nodes to the dry node. The gravitational force has to be preserved. To distinguish between those two situations, the method proposed in [7] compares the maximum value of the surface elevation with the minimum bathymetry on the element: $s = \max(\eta) + \min(h)$. When the value of s is smaller than a given

threshold ε, the gravity is cancelled on the element. This procedure guarantees that the mean water depth H over each element will be positive at the end of one time step. An additional slope-limiting algorithm is applied locally on each element to guarantee a positive depth at the nodes.
To be usable in an implicit temporal scheme, this on/off switch has to be regularized. In order to do so, we multiply the gravitational fluxes between the nodes of a partially dry element by a blending parameter α, defined according to Eq. (3). When the value of s is less than a threshold value ε, the blending parameter α is 0 (see Fig 2(a)). When the value of s is larger than 5ε, the blending parameter α is equal to unity (see Fig 2(b)). In other situations, α is interpolated from 0 to 1. The following formula is used:

$$\alpha = min\left(1, max\left(0, \frac{s-\varepsilon}{4\varepsilon}\right)\right) \tag{3}$$

In addition, the water depth is limited to ε_2 in the bottom drag and wind stress parametrization to avoid unrealistic forcing. We use $\varepsilon_2 = \varepsilon$ in the three test cases below.

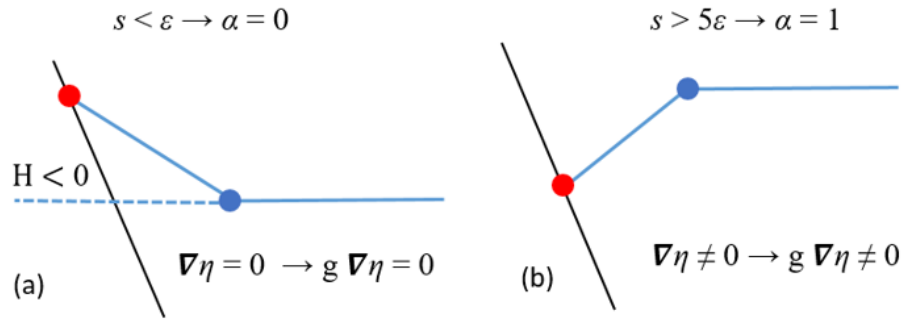

Fig. 2 Evolution of free surface when using a blending parameter: (a) s is smaller than the tolerance value and (b) s is higher than the tolerance value; bottom (black line), water surface (blue line), water surface in dry cell (dashed line) and cell nodes (dots).

In comparison with other wetting - drying algorithms implemented in SLIM, our work presents several novel contributions. For example, in the explicit algorithm by [11], the key ingredient was the use of limiters for generalized nodal fluxes. The method by [10] applied to implicit time schemes. It was developed for artificial displacements of sea-bed positions in drying areas. The Balzano testcase 3 reveals that water is leaking through dry areas which can be seen as a drawback of his method. Our model uses implicit time schemes that can significantly reduce computational cost. It applies a thin - layer method and a blending parameter for a smooth transfer from dry to wet states near the wetting front. Global and local mass conservations are guaranteed.

2.4 Validation of the algorithm

In this section, the performance of the proposed algorithm is assessed on the basis of several test cases. Below, all the values of the variables are expressed in the International System of Units, i.e. m (meter), s (seconds) etc. The discrete initial conditions and the bottom topography are derived from the analytical ones by interpolation at the nodal (cell interface) points.
We selected the Balzano 1, Balzano 3 and Thacker testcases for our algorithm validation because the Balzano 1 testcase is the simplest one in the set of three simple testcases introduced by Balzano [29] with an uniform slopping bed. The Balzano 3 testcase is the most difficult one in this set. It includes of a small reservoir, allowing to check whether or not water will leak into the rest of the basin. Thacker testcase is to simulate water oscillation in a paraboloid bowl. The Balzano 3 testcase and Thacker testcase are here of use to illustrate that the method is strictly mass conserving.

2.4.1 The Balzano 1 test case

The first of three idealized 1D test cases developed by Balzano [29] is widely used to evaluate the accuracy of various wetting - drying methods [30] because they exhibit problematic conditions in a simple setup [19]. Originally, the computational domains of these three Balzano test cases are 1D basins with a length of 13800 m. However, as the purpose of this paper is to test the implementation of the new wetting - drying algorithm in the 2D version of SLIM, these domains are modified by adding a width of 7200 m. It is then verified that the solutions of the 2D simulations performed by means of SLIM on unstructured meshes correspond to the 1D solutions of the original Balzano test cases.
In all Balzano test cases, the Coriolis force, the surface stress and the horizontal viscosity are not taken into account. The simulation time step is 1 s. The only difference between the three test cases is the bathymetry.
The first Balzano test case aims at simulating a wave run up on a basin with a uniform bed slope (see Fig. 3). The undisturbed water depth is $h = x/2760$, where x is the coordinate in the main direction of the basin.
The threshold thickness ε is a key issue in the wetting - drying algorithm. Mass conservation should be satisfied and the computational cost needs to be affordable. As the Balzano 1 test case is a simple one, it is possible to run it with different value of ε to investigate the sensitivity of the results to these values. The width and length of the domain are kept identical for all simulations while the slope is modified with the depth varying from 3 to 50 m corresponding to variations of ε in a range of 0.001 - 1 m. Fig.4 shows the relation between ε and the reference depth. It is clear that the value of ε should be increased as the depth increases. The blue dots indicate the runs where the simulation can work with ratio of ε/depth exceeding 0.2 %. If the ratio is smaller than 0.2 %, the non-linear Newton - Raphson solver does not converge. Therefore, the threshold value ε is selected to be 0.01 m for all test cases.
In the first Balzano test case, a sinusoidal water level variation is imposed at the open boundary (x = 13800 m) with a period of 12 h and an amplitude of 2 m. Our model results are in agreement with previous publications such as [11,10, 29]. According to the summary by [31], some schemes cause unintended problems,

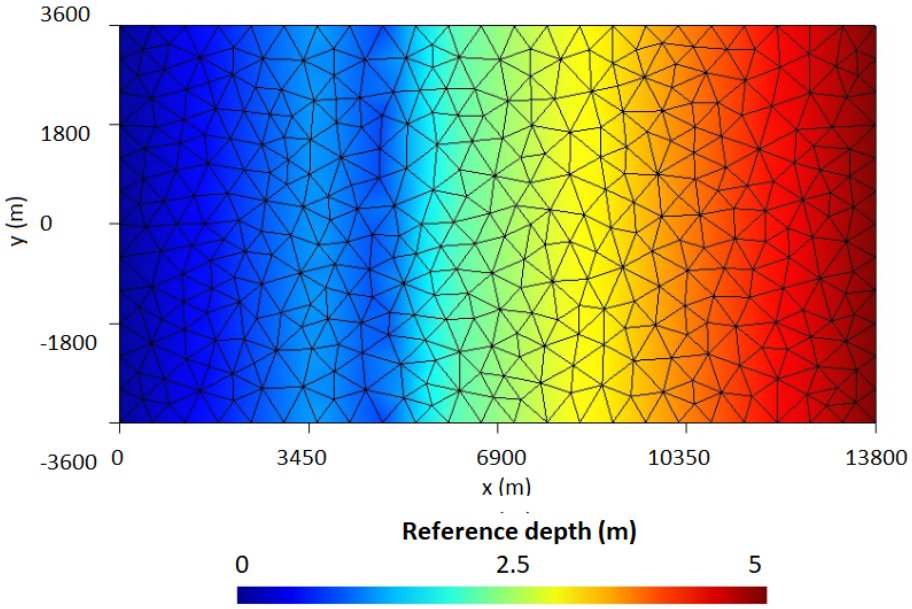

Fig. 3 Mesh with 500 m edge size and 716 triangular elements used for the Balzano 1 test case

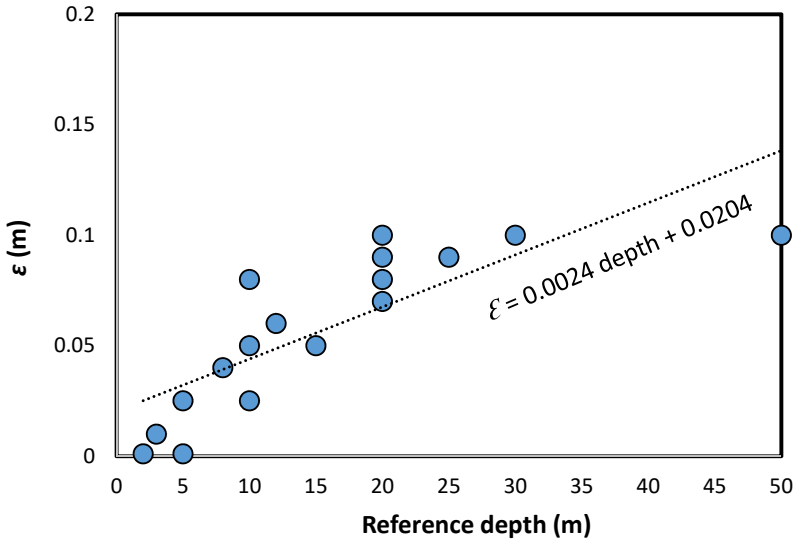

Fig. 4 The relation between the minimum value of ε and the reference water depth for the mesh illustrated in Fig. 3

for examples wiggles in the free surface profile during the wetting phase and in the drying phase, and pronounced underestimation (negative water thickness) or overestimation (positive water thickness) in the retention volume. By applying the proposed algorithm in SLIM, with the threshold value ε, the water thickness remains always positive and limited in dry areas (see Fig. 5), the retention volume is never underestimated, and the overestimation is controlled.

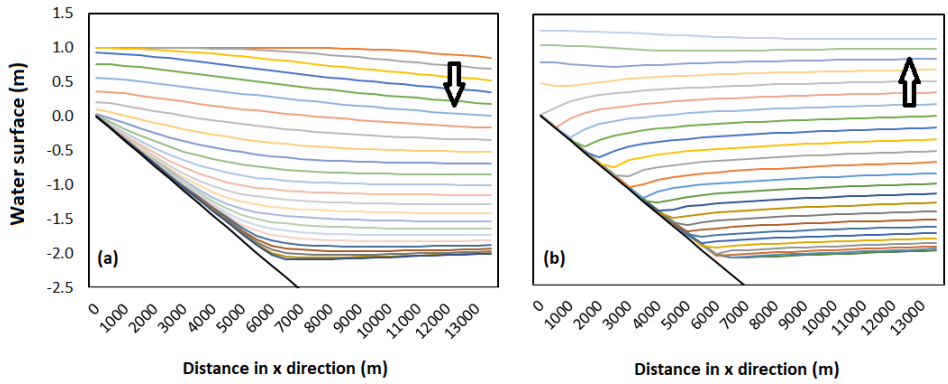

Fig. 5 First Balzano test case: vertical section through the domain of interest, showing the bottom (black line) and the water surface evolution every 600 s (colour lines), during the drying (a) and the wetting (b) phases with downward arrow and upward arrow, respectively.

2.4.2 The Balzano 3 test case

The same simulation as the Balzano 1 test case is repeated but with a modified bathymetry. The new bathymetry contains a small reservoir that can retain water in the drying phase (see Fig. 6). The analytical expression of the bathymetry is as follows:

h = x/2760 if x $\leq$ 3600 m or x $\geq$ 6000 m
h = 30/23 if 3600 m $\leq$ x $\leq$ 4800 m
h = x/1380 - 50/23 if 4800 m $\leq$ x $\leq$ 6000 m

The mesh comprises 706 triangular elements of uniform size with edges of about 600 m. A sinusoidal water level variation is imposed at the open boundary with an amplitude of 3 m initially. The free surface elevation at the open boundary decreases from 3 to -3 m at the open boundary after 12 h of simulation. Then, water level is kept constant for an indefinitely long time in order to test whether water is leaking through the dry area, out of the small intermediate basin. Indeed, with some wetting - drying methods, some water can flow from the reservoir to the rest of the basin, even when the mean surface level inside the reservoir is below the local peak of the bathymetry. Here, after 36 h of simulation, the expected water level is maintained in the reservoir. The physics does not seem to be altered at the boundaries between wet and dry areas. The simulation ends after 48 h and confirms that no negative water thickness appears in the whole domain.

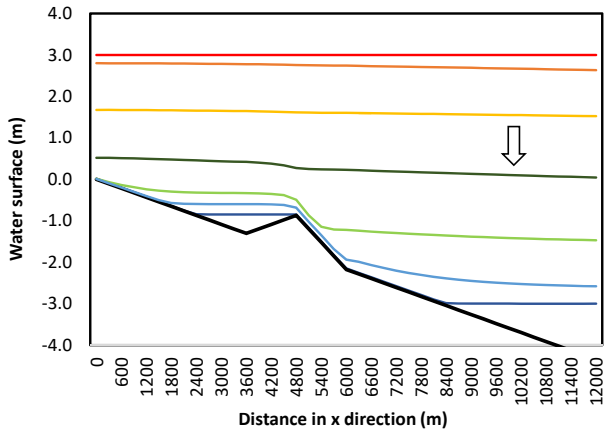

Fig. 6 Third Balzano test case: vertical section through the domain of interest, showing the bathymetry (black line) and the water surface evolution at the initial condition (red line) and equilibrium (blue line) by arrow

2.4.3 The Thacker test case

This last test case has also been used by [29] to compare the best methods of his review, and also e.g. by [11,10,32,7]. It reveals if a method is strictly mass conservative. The domain is a circular closed basin with a radius $R = 430.62$ km, so that no water can enter or leave the domain; the bed is a paraboloid of revolution. At the initial time, the free surface is also a paraboloid of revolution.
The free surface moves with periodical oscillations and wetting - drying occurs in the vicinity of the outer boundary of the domain. In the absence of the Coriolis force, surface stresses and dissipation (neither viscosity nor bottom stress), the analytical solution for the non-linear shallow water equations is known [33]. Here, the mesh is generated with a size gradually increasing from 10 km near the boundary to 30 km at the center. The total number of triangles is 14114. The simulation time is 72 hours (256,200 s), corresponding to 6 periods, allowing for a good assessment of the water surface evolution in the basin. Water depth in the center of the basin at rest is $h_0 = 10$ m and initial surface water elevation is $\eta_0 = 2$ m. The unperturbed water depth and the free surface elevation are as follow:

$$h = h_0 \frac{R^2 - r^2}{R^2} \tag{4}$$

$$\eta = h_0 \left(\frac{\sqrt{1 - A^2}}{1 - A\cos\omega t} - 1 - \frac{r^2}{R^2} \left(\frac{1 - A^2}{(1 - A\cos\omega t)^2} - 1 \right) \right) \tag{5}$$

with

$$\omega^2 = \frac{8gh_0}{R^2} \tag{6}$$

$$A = \frac{(h_0 + \eta_0)^2 - h_0^2}{(h_0 + \eta_0)^2 + h_0^2} \tag{7}$$

where r is the radial coordinate ($r = 0$ at the center of the domain).

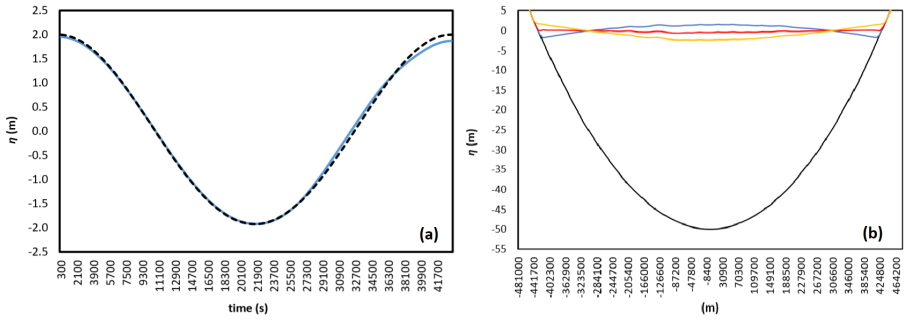

Fig. 7 Thacker test case: (a) Comparison of water surface elevation in the domain center: with the dashed line representing the analytical solution and the continuous blue line representing the numerical solution; (b) Vertical section showing the sea bed (black line) and position of simulated water surface at initial time (blue line), after 3 hours (red line) and after 6 hours (orange line)

.

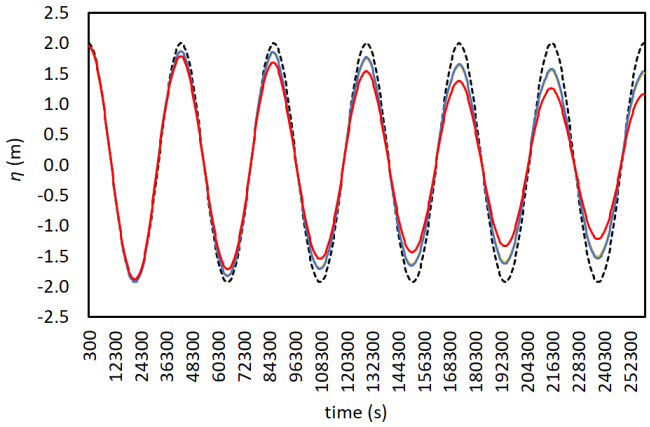

Fig. 8 Thacker test case: Evolution of water surface elevation in the domain center with different time steps: dash black line is the exact solution of Thacker, assuming zero dissipation; blue line (dt = 1 s), orange line (dt = 10 s) and red line (dt = 100 s)

An adequate time step should be selected to capture the physics of interest. The threshold thickness ε is fixed to 0.01 m and the simulation time step is 1 s. The analytical expressions of the bathymetry and the solution of the non-dissipative problem are given by equation (4) - (7). However, the proposed wetting - drying method, by using an implicit time integration, introduces some numerical dissipation. It is depicted in Fig. 7 showing the time evolution of the water level at the centre of the basin: overall, there is a fairly good agreement between the numerical solution and the analytical solution. The evolution of the free surface elevation at the center of the domain during 72 hours is shown in Fig. 8.
The mass conservation is assessed for 3 simulations with 3 different time steps. The results confirm 100 % of mass conservation for time step of 1 s. Less than 0.001 % of mass is lost after 72 hour simulation with time steps of 10 s and 100 s.

3 Application to the Tonle Sap

The proposed wetting - drying algorithm has been assessed by several analytical test cases, showing that the scheme is well-balanced, mass conservative and stable for rapid transitions of the wet/dry interface with different time steps of 1 s, 10 s and 100 s. However our scheme is not strictly momentum conservative. We clipped the velocity in partially dry elements and had additional dissipative terms such as viscosity, bottom drag and wind stress parameters ε_2. Thus it can be applied for flash flooding condition and dam break flow. Hopefully, the proposed technique is a robust method, which is able to handle realistic and complex water bodies. It is seen below that it can simulate the inundation process and subsequent drying in the Tonle Sap lake, Cambodia floodplain.

3.1 Study area

The Tonle Sap is an important water body, located in the Cambodian floodplain which contributes largely to the Mekong river dynamics [34]. It comprises a permanent lake, 12 tributaries, extensive floodplains and the Tonle Sap River linking the lake to the Mekong River. The permanent lake extends over of a large territory towards the Northwest of Cambodia, with dimensions of 75 km x 32 km. It comprises a small part in the Southeast of the domain with dimensions of 35 km x 28 km [35, 36]. The lake and its floodplains form the largest freshwater source in Southeast Asia [34]. The Tonle Sap River with a length of approximately 120 km [37] is situated at the Southeast end of the Tonle Sap lake and joins the Mekong River at Chaktomuk confluence. At the confluence, the river splits into the Bassac River in the West and the Mekong River in the East.
The hydrology of the Tonle Sap is driven by the monsoonal flood regime of the whole Mekong River Basin [38, 39]. As a result, the Tonle Sap has a unique hydrological regime. In the flooding season (from June to October), when the water level of the Mekong River is higher than in the Tonle Sap lake, reserve flows takes place from the Mekong River into the lake. In addition, discharges from the 12 tributaries and overland flow provide additional water sources for the lake. Therefore, the water level in the lake increases from 1.44 m to 9.09 m [34]. At the beginning of the dry season (November), the water level in the Tonle Sap lake reaches a peak value and its level becomes higher than the level in the Mekong River. Thus the flow changes its direction and water discharges from the Tonle Sap lake towards the Mekong River. Hydrologically, the lake functions as a regulatory reservoir for the Mekong Delta of Vietnam [36, 40], storing approximately 50 % of total Mekong inflow and releasing 90 % of outflow to the Mekong River [41], providing a freshwater inflow to the downstream region in dry season [42]. With this phenomenon, the flooded area varies from 7,190 to 12,720 km^2 [34] and causes the occurrence of dry areas after water recedes. This specific hydrological behavior is vital for all the riparian communities [34].
The new wetting - drying algorithm integrated in SLIM is used to simulate the complex flow regime in the Tonle Sap. The computational domain extends over the floodplains, and is limited to the south at Phnom Phenh, at the confluence with the Mekong River at Chaktomuk. Among other coordinate systems utilized for hydrodynamic modelling, such as the Geographical coordinate system, the Carte-

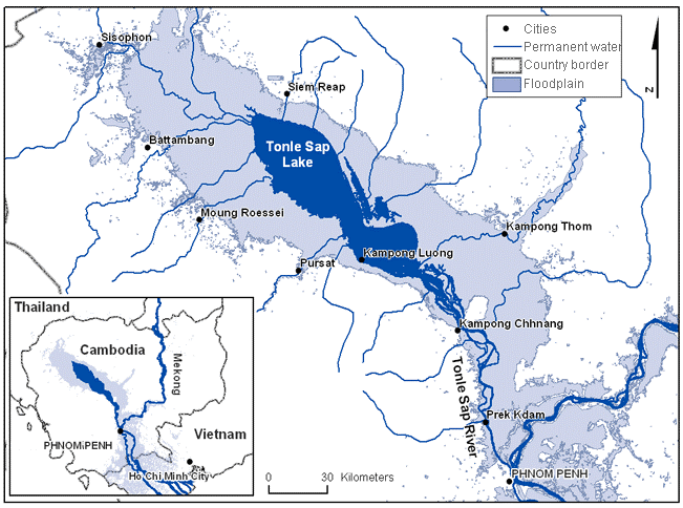

Fig. 9 Map of the Tonle Sap system and its sub-catchments [48]

Table 1 Sub-catchments of Tonle Sap [50]

No.	Sub-catchment	Area (km^2)
1	Chinit	8236
2	Sen	16359
3	Staung	4357
4	Chikreng	2714
5	Siem Riep	3619
6	Sreng	9986
7	Sisophon	4310
8	Mongkol Borey	10656
9	Sangker	6052
10	Dauntri	3695
11	Pursat	5965
12	Boribo	7153
	Lake (average)	2887
Sum		**85,989**

sian coordinate system and the Curvilinear coordinate system [43], our model uses a Universal Transverse Mercator (UTM) coordinate system because of its small distortions. The multi-scale mesh is generated by the algorithm developed by [44, 22]. The mesh consists of 187,906 triangular elements with 94,544 nodes. The finer mesh elements are used to represent the 12 tributaries and the Tonle Sap River while the coarser mesh elements are used for the floodplains and the permanent lake. The mesh resolution varies from 200 m to 2000 m in order to take into account the wide range of physical processes occurring in the computational domain. The application of this multi-scale mesh allows to simulate both small-scale and large-scale processes within a single model without nesting [26]. Our model does not take into account the interaction between groundwater and surface water because [34] it is estimated that groundwater discharge to the lake is approximately 4 - 8 km^3 per year, accounting for only 5 - 10 % of total annual inflow.

3.2 Model set up

The bathymetry of the computationa domain was constructed from two data sets. First, the topographical data was obtained from the Mekong River Commission (MRC, 2003) under the form of a Digital Elevation Model (DEM) with a 50 x 50 m grid resolution. Then, local cross-section measurements done by the Mekong River Commission provide a description of the bed elevation in the lake and the river. The bathymetry of the lake is very irregular with variations from - 50 to 0 m. Value 0 is the origin of the vertical axis at the bottom of the lake. The negative values of the vertical coordinate mean the topographical elevation (Fig. 10). The daily discharge from the 12 tributaries and the daily water level at Phnom Phenh (downstream boundary) are imposed at the boundaries of the computational domain (Fig. 11). These data (Fig. 12) were obtained from the Mekong River Commission. No-slip and impermeability conditions are set along the close boundaries. The downstream open boundary condition consists of the water level variation measured at Phnom Phenh.
Daily water level measurements at Kompong Luong station, located in the lower part of the lake; and at Prek Kdam, located in the Tonle Sap River, are presented in Fig. 13; they are used here below for model validation. These data are collected from the monitoring network of the Mekong River Commission since 1994 to present. The numerical simulations are performed to determine (1) the spatial and temporary fluctuations of the Tonle Sap flow as well as the changes in water level and inundated area of the Tonle Sap system; and (2) the hydraulic relation between the Tonle Sap and the Mekong River.
To cope with the large bathymetry gradient in this real topography, the water velocity on partially dry elements is clipped to 0.1 m/s. The thresholds for advection parameter ε_2 and drag parameter ε_3 are set to be 2 m and 0.5 m, respectively.

3.3 Results and discussion

3.3.1 Model calibration and validation

The hydrodynamic modeling of a natural domain requires a careful selection of parameters (e.g the Manning coefficient) to simulate the physical conditions as closely as possible to real conditions. In addition, the parameters of the implicit wetting - drying algorithm must be calibrated to maintain numerical stability and a reasonable simulation time.
Model calibration and validation are performed by comparing the water level observed at Kompong Luong and Prek Kdam stations and with simulated ones (see Fig. 10). Then using the calibration model, the filling and emptying processes of the lake is analysed for two extreme situations: a dry and a wet year. The calibration period is selected from 1/5/2009 to 30/4/2010 and the validation period is from 1/5/2008 to 30/4/2009 because these periods are representative for normal hydrological conditions (see Fig. 13). The numerical results will be compared to observed water levels at these two stations. The Manning coefficient is used for parameterizing the bottom friction. From the calibration simulations with different Manning coefficients (n = 0.032 s/m$^{\frac{1}{3}}$, 0.035 s/m$^{\frac{1}{3}}$ and 0.038 s/m$^{\frac{1}{3}}$, see Table 2), the optimal one was found to be n = 0.035 s/m$^{\frac{1}{3}}$ in the whole domain, which

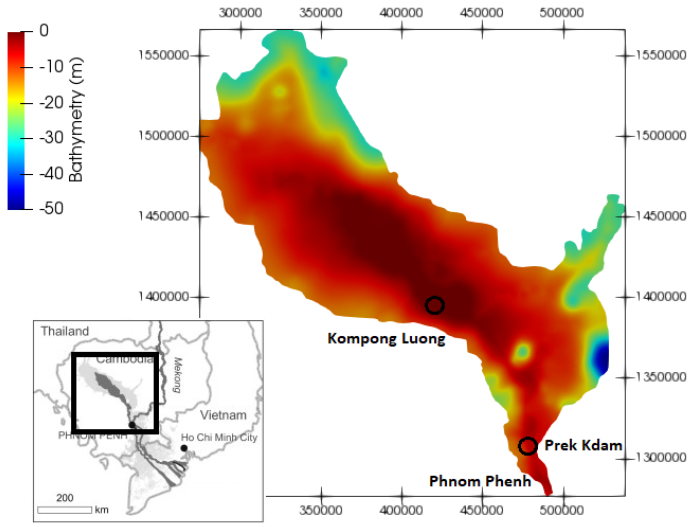

Fig. 10 Location and bathymetry of the domain with Kompong Luong station and Prek Kdam station. In this domain, value of 0 is the origin of the vertical axis at the bottom of the lake. The negative values of the vertical coordinate mean the topographical elevation.

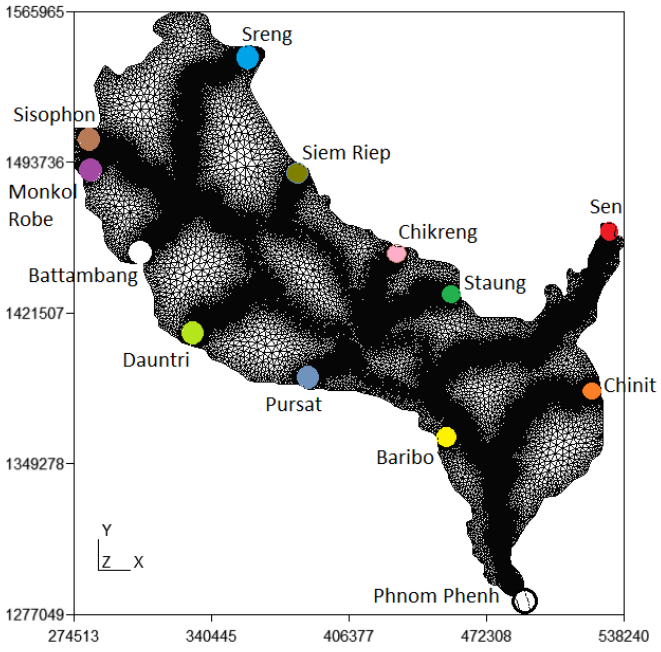

Fig. 11 Computational mesh. The color dots show the 12 stations corresponding to the tributaries as water inputs and the white dot represents the downstream boundary of the model at Phnom Phenh station.

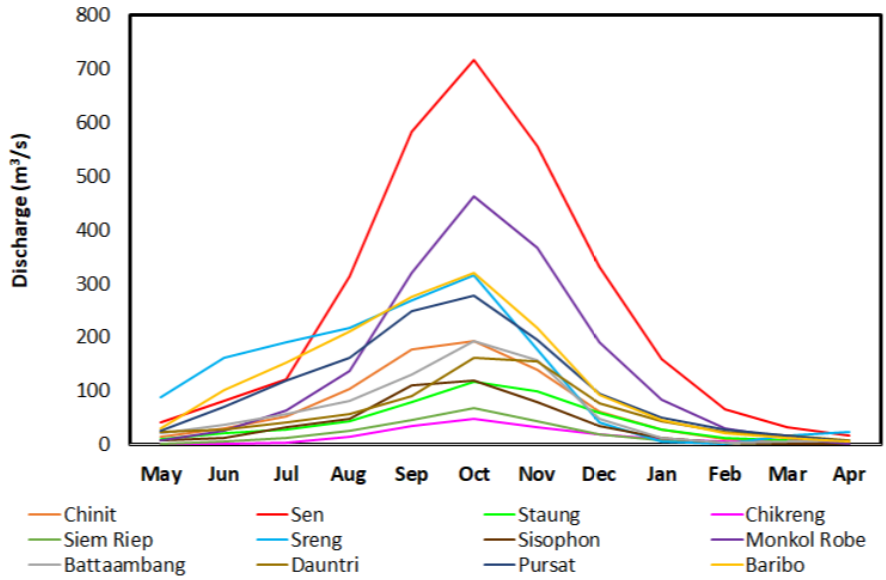

Fig. 12 Monthly averaged discharge at the 12 stations indicated in Fig. 11

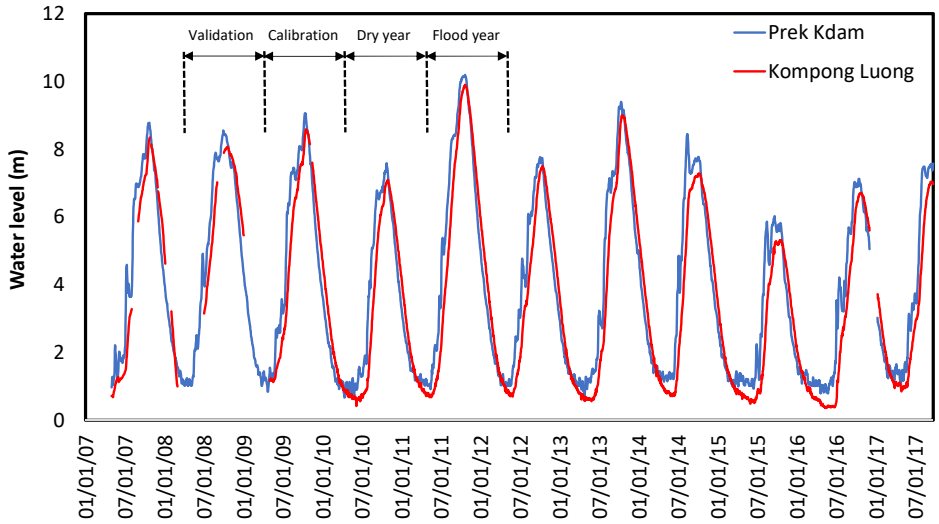

Fig. 13 Water level at Kompong Luong (red line) and Prek Kdam (blue line) for years 2006 - 2017

is in a good agreement with previous studies [40,45]. The threshold value of water depth ε for the wetting - drying algorithm is selected by the method applied in the Balzano test case 1 and considering the computation cost. It is fixed to be 0.1 m. With the high detailed mesh and the computation time step of 300 s, it takes approximately 20 days for simulating a hydrological year by 16 parallel processors at 2.0 GHz and 64 GB of RAM.
The quantitative assessment of the results for each tested value of the parameters is achieved using the Nash-Sutcliffe coefficient (NSE):

$$NSE = 1 - \frac{\sum_{n=1}^{n}(H_{obs,i} - H_{simu,i})^2}{\sum_{n=1}^{n}(H_{obs,i} - \overline{H}_{obs})^2} \tag{8}$$

where $\overline{H}_{obs}$ is the mean value of observed waterdepths, $H_{obs,i}$ is the observed water depth at time t = i Δt and $H_{simu,i}$ is the numerically simulated water depth at time t = i Δt, n being the total number of time steps.
The mean absolute error (MAE) is applied to measure the absolute differences between simulated results and observations:

$$MAE = \frac{\sum_{n=1}^{n}|H_{obs,i} - H_{simu,i}|}{n} \tag{9}$$

In addition, the Root Mean Square Error (RMSE) is also used to evaluate the quadratic average difference between computed results and observed data.

$$RMSE = \sqrt{\frac{\sum_{n=1}^{n}(H_{obs,i} - H_{simu,i})^2}{n}} \tag{10}$$

The summary of model validation is shown in Table 2 and Fig. 14 and Fig. 15. The numerical results are in good agreements with observed data. The validated parameters will be applied for testing different scenarios in severe conditions, for the flooding year 2011 and dry year 2010 as described below.

Table 2 Model validation

	Kompong Luong		**Prek Kdam**	
n = 0.032 s/m$^{\frac{1}{3}}$	Calibration	Validation	Calibration	Validation
RMSE (m)	0.70	0.90	0.36	0.23
MAE (m)	0.53	0.79	0.27	0.18
NSE (%)	92.56	63.78	98.31	99.23
n = 0.035 s/m$^{\frac{1}{3}}$	Calibration	Validation	Calibration	Validation
RMSE (m)	0.61	0.30	0.41	0.22
MAE (m)	0.29	0.23	0.34	0.23
NSE (%)	94.63	95.97	97.70	99.36
n = 0.038 s/m$^{\frac{1}{3}}$	Calibration	Validation	Calibration	Validation
RMSE (m)	0.66	0.85	0.21	0.21
MAE (m)	0.26	0.73	0.56	0.73
NSE (%)	93.44	67.71	98.03	99.36

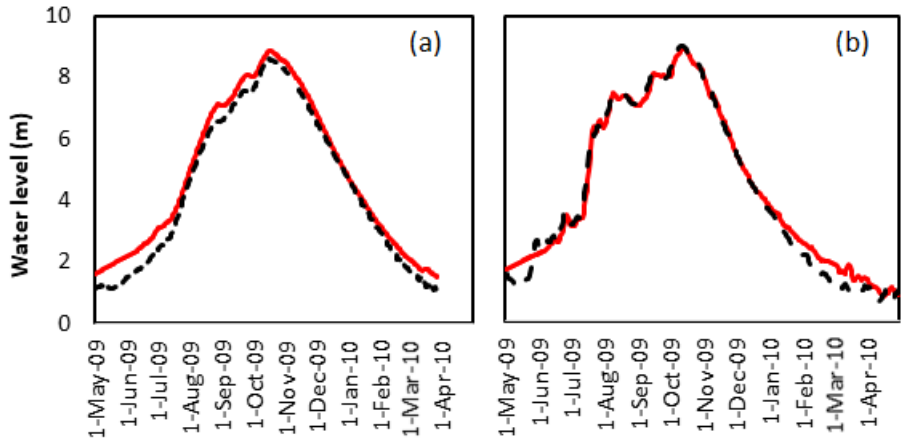

Fig. 14 Calibration of water level in Kompong Luong station (a) and Prek Kdam station (b) from 1/5/2009 to 30/4/2010. The red continuous line corresponds to the simulated results and the dashed black line corresponds to in situ measurements.

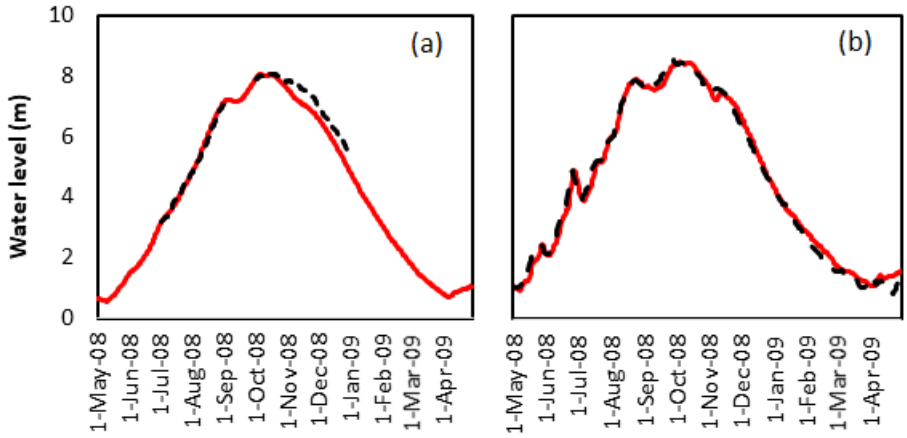

Fig. 15 Validation of water level in Kompong Luong station (a) and Prek Kdam station (b) from 1/5/2008 to 30/4/2009. The red continuous line corresponds to the simulated results and the dashed black line corresponds to in situ measurements.

3.3.2 Filling and empyting of the lake: Flood pattern 2011

The hydrological year 2011 (May 2011 until April 2012) is selected because this year is regarded as historically extreme for both the spatial extent area and the water depth of this seasonal inundation across the Cambodia floodplain and the Mekong Delta of Vietnam [45] (see Fig. 13) during 88 years of observation [46]. Simulation results are illustrated in Fig. 16, where the extent of the inundated area as well as the representative depth-averaged velocities are illustrated for each month. The wetting - drying process can be clearly identified: panels (a) and (b)

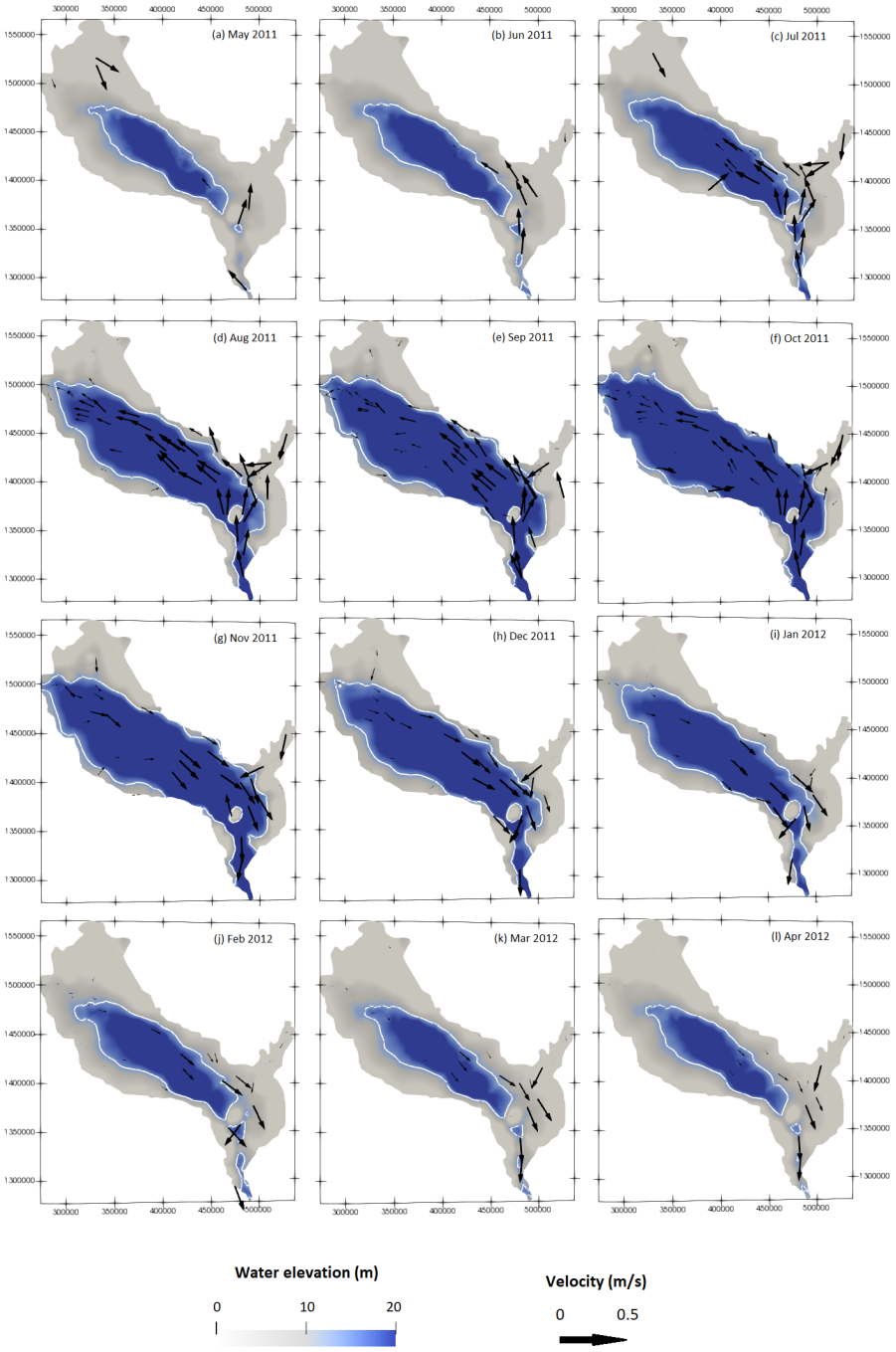

Fig. 16 Surface water area and flow patterns simulated for the extreme flood year 2011

are a transition period of dry - wet seasons; panels (c), (d),(e), and (f) are months of the wet season; panels (g), (h), (i), (j) and (k) are months of the dry season. The blue colour shows wet areas and gray colour shows dry areas. The arrows illustrate representative current magnitudes and directions. The white line is the limit of the wet areas. So, a flooding and dewatering pattern can be observed, as a result of water depth fluctuations with respect to the real topography.
Fig.16 (a) represents the results for May 2011. This month is the end of the dry season and the beginning of the flood season, so there are relatively large dry areas, which are located almost over the whole domain. Only the permanent lake is flooded with a maximum water depth of 10.66 m, a mean water level of 1.06 m and a wet area of 1528 km^2. The southern part of the domain has the lowest bed elevation, thus the water flows from this point in the northwestern direction to the lake and starts filling up the domain. Flows from the northern tributaries also begin reaching the lake. Thus the wet area extends gradually.
Fig. 16 (b) shows the situation of June 2011. This month is the beginning of the wet season. The lake has inflow and outflow, however the prevailing direction is flow towards the lake. Together with flows from tributaries, the flow from the Mekong river makes water level rise sharply to 2.21 m and the wet areas expand on both sides of the lake. Vectors representing current flow clearly show the dominance of water discharge from the Mekong river to the lake.
In Fig. 16 (c) for July 2011, the water level rises up to nearly 4.36 m, with an inundated area of approximately 6328 km^2 and the input water of the lake is strongly sourced from the Mekong river and its tributaries. Fig. 16 (d) and Fig. 16 (e) correspond to August and September 2011, which are in the middle of the wet season. Therefore, the water depth is very high with values of approximately 8.90 m. The prevailing flow direction is from the Mekong river towards the lake and the dry areas are getting smaller.
October is the end of wet season, as shown in Fig. 16 (f); the water level reaches its peak at 9.98 m and the maximum inundated area is about 13,329 km^2. Approximately 90 % of the floodplain area is covered by water at the peak level. The dry areas are only located in the north, east and mountain of the whole domain. At the end of this month, when the water level in the lake is higher than in the river, the flow starts changing its direction, toward the Mekong river. The current is the strongest at Prek Kdam.
November - April is the dry season and thus the related panels show outflow from the lake, see Fig 16 (g) - Fig 16 (l), the water levels and surface areas reduce gradually to the minimum levels of 1.14 m and 1726 km^2, respectively, exactly in April 2012. Based on the topographical condition, the northern part of the lake is getting dry first while the southeast part is always wet and flow in this area is strongest.

3.3.3 Filling and empyting of the lake: Dry pattern 2010

According to the observed data from [46,45] and Fig. 13, year 2010 (May 2010 to April 2011) is the driest year in the observation period. This simulation is implemented to reproduce the surface area and flow panels in comparison with the flood year. Similarly to year 2011, the period of May - October is the wet season, and the period of November - April is the the dry season. From May to July 2011 (see Fig 17(a), Fig 17(b) and Fig 17(c), the main water sources of the lake

originate from the Mekong river and the Tonle Sap's tributaries. Thus water level in the lake varies gradually from 0.95 - 1.74 m, the wet area increases to 2,775 km^2 at the end of July 2011. From August to October 2011, the lake receives water from two sources, mainly from the Mekong river and a partly from its tributaries. Sen is a major tributary of the Tonle Sap because of its large area and high discharge (see Table 1 and Fig. 12). Thus it plays an essential role supplying water for the Tonle Sap. After this period, the water level goes up to 7.48 m, corresponding to an area of 10,208 km^2. The period of November - April corresponds to the dry season, thus the water level and surface area reduce sharply to the minimum values of 1.15 m and 1750 km^2. The variations of water level, surface area and water volume between 2010 and 2011 are presented in Table 3.

3.4 Discussion

3.4.1 Variation of Tonle Sap characteristics in a year

According to the observed hydrographs of the Mekong River and of the 12 tributaries of the Tonle Sap, and to the diagrams of water level evolution in the lake, four distinct phases can be identified in the flood regime of the lake: (1) the rising phase (May - August), when the water level rises fast and water occupies larger areas; (2) the wet phase (September - November), when the water level grows slowly and the changes of inundated area are no more significant; (3) the receding phase (December - February), after the peak water level records, when the water levels significantly decreases as well as the flooded area; and (4) the dry phase (March - April), when the water level and flooded area reduce again to minimal values.

During the simulation of the flooding year (2011), the inundated area has increased by 11,628 km^2 from 1,503 km^2 (mean value) to a maximum value of 13,329 km^2, corresponding to a variation of the water level between 1.06 m and 9.98 m. As a result, a large area is exposed to transitions from dry to wet condition and vice-versa. Similar features are observed during the dry year (2010), as the inundated area has increased by 9,114 km^2 from 1,200 km^2 to a maximum value of 10,314 km^2, corresponding to a variation of water level between 0.95 m and 7.51 m. This result confirms the close relation between the flood-pulse features of the Tonle Sap Lake and flooding - dewatering phenomena, which are under the direct impact of the flow from the Mekong mainstream [47, 48, 34].

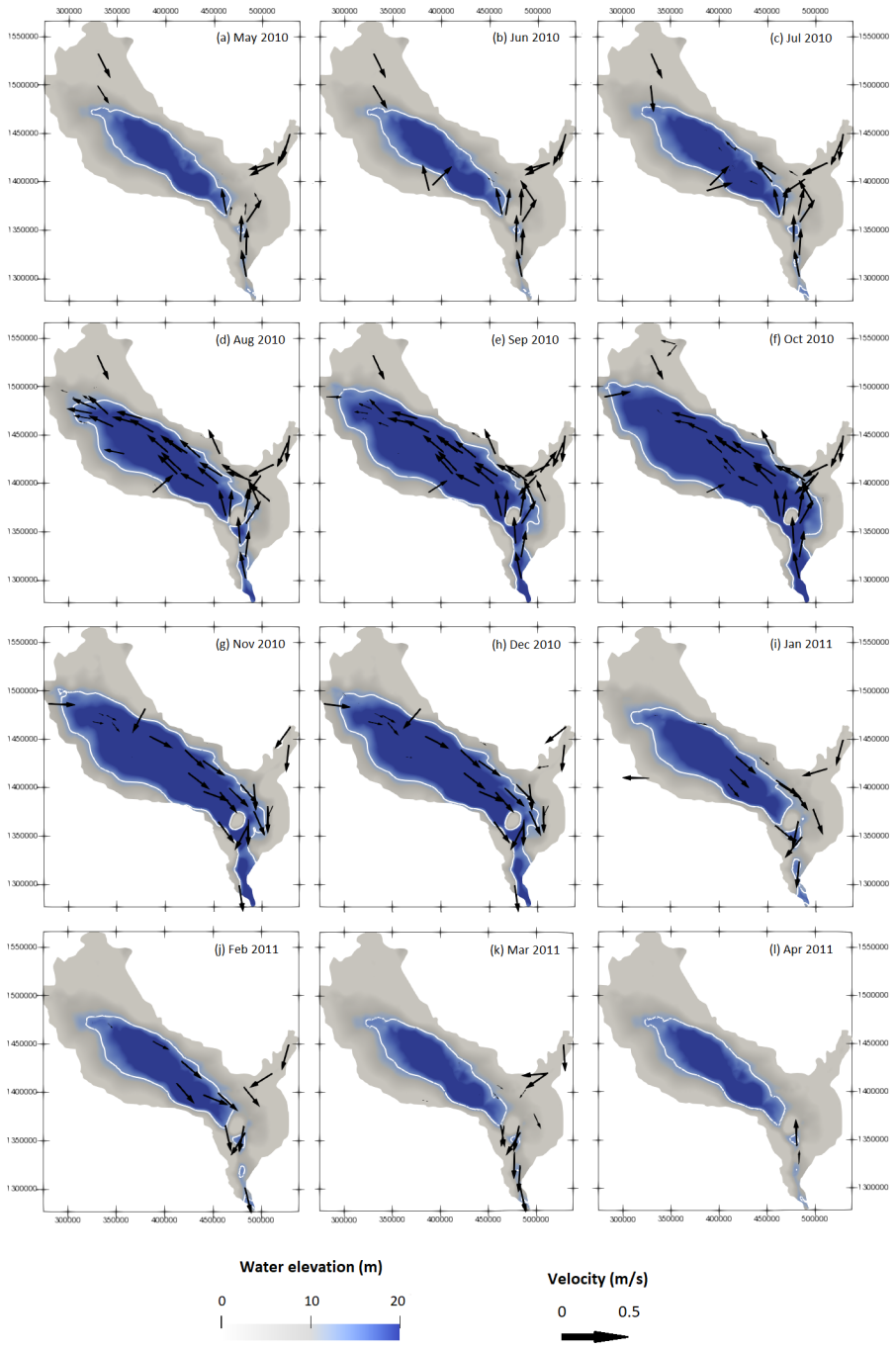

Fig. 17 Surface water area and flow patterns in dry year 2010

3.4.2 Variation of Tonle Sap characteristics during flood and dry years

Regardless of the type of flow conditions (flooding year or dry year), the hydraulics of the Tonle Sap presents key features related to the flow driven by the Mekong River. According to simulated results, during both considered years, significant monthly variations are observed from the beginning of the wet season and reach a peak in October, then the observed values reduce until the end of the dry season (see Fig. 18 and Table 3). However, the amplitude of the phenomena differs: in October, the highest water level and surface area of year 2010 (dry year) are 77 % of the same values recorded in year 2011 (flooding year), while the maximum water volume in 2010 corresponds to less than 58 % of that in 2011.

Table 3 Variation of lake characteristics between 2010 and 2011

	Dry year 2010	Flood year 2011	Difference
Min level (m)	0.95 *(11 May 2010)*	1.06 *(12 May 2011)*	0.10
Max level (m)	7.51 *(01 Nov 2010)*	9.98 *(22 Nov 2011)*	2.47
Level variation (m)	6.56	8.92	2.37
Min area (km^2)	1,200	1,503	203
Max area (km^2)	10,314	13,329	3,015
Area variation (m^2)	9,114	11,628	2,712
Min volume (mill. m^3)	223	356	133
Max volume (mill. m^3)	40,674	69,916	29,242
Volume variation (mill. m^3)	40,451	69,560	29,109

3.4.3 Flow contribution

The monthly discharge at Prek Kdam is calculated from SLIM results and compared with the measured discharge at Phnom Phenh; and with the total discharge from 12 tributaries of the Tonle Sap (Fig. 19). The monthly discharge at Prek Kdam shows two groups of values. The negative values mean inflow from the Mekong River towards the lake, that occurs during the wet season. The maximum monthly value is approximately 7100 m^3/s. The positive values start from November to April, meaning that the flow is outward. The maximum monthly value is about 5000 m^3/s, approximately 2100 m^3/s lower than in flood season. It can be explained by the contribution of flow from tributaries and the lakes retention capacity. The minimum monthly flow appears in April with value of approximately 750 m^3/s. At this time flow from the Tonle Sap is the main water source supplying the Mekong Delta. The discharge from Phnom Phenh and the total discharge from the 12 tributaries show the time lag with maximum value in September and October, respectively. As the amplitude of the discharge at Phnom Phenh is 10 - 20 times higher than the one of the tributaries, it confirms the flow pulse of the Tonle Sap is dominated directly by the flow regime from the Mekong river under the cyclic episodes of flooding and drying. This outcome is consistent with [49,34].

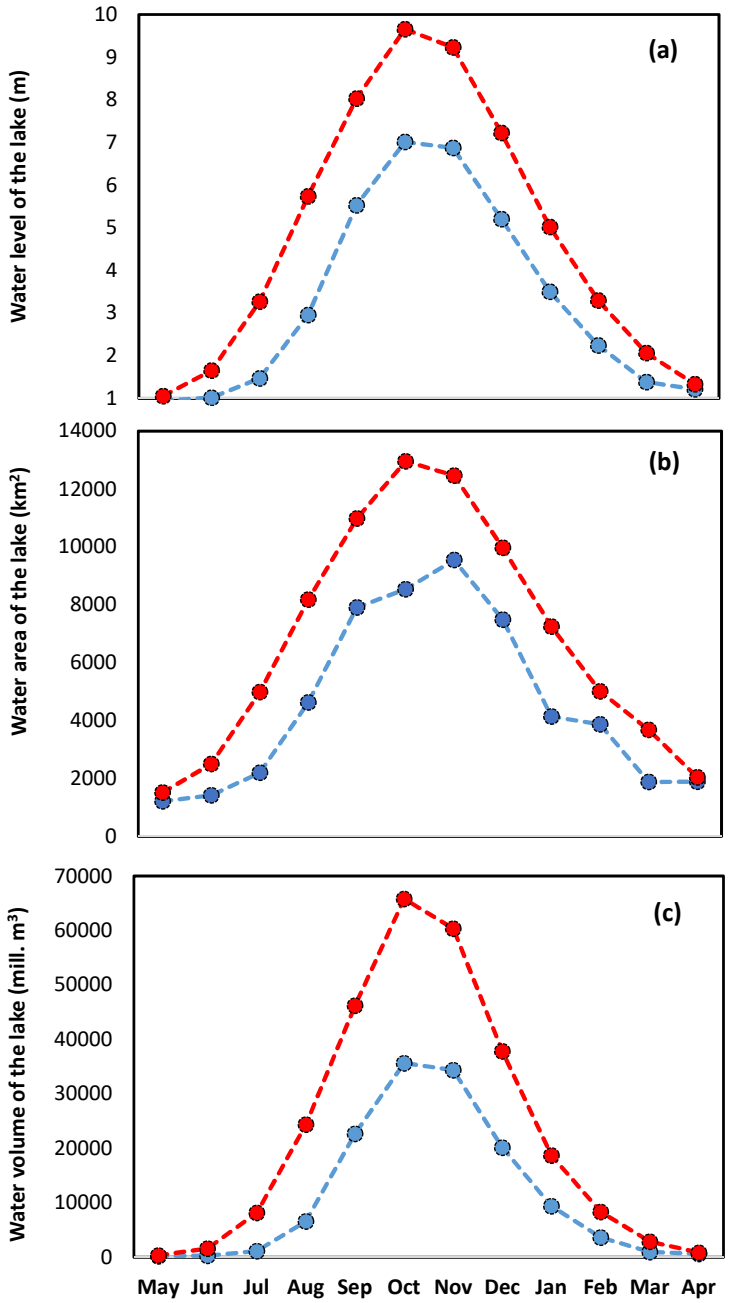

Fig. 18 Variation of water level (a), surface area (b), water volume, (c) between flooding year (red) and dry year (blue) in the Tonle Sap lake

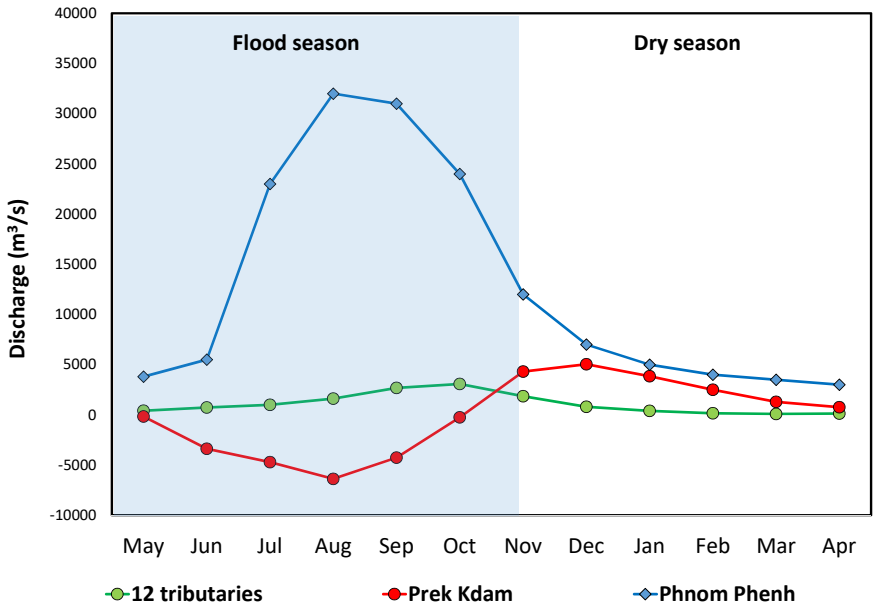

Fig. 19 Mean monthly discharge at Phnom Phenh (blue - measured) and total discharge from 12 tributaries of the Tonle Sap (green - summary) in comparison with discharge at Prek Kdam (red - simulated) for the period 2008 - 2012

3.4.4 Comparison with previous studies

To confirm the accuracy of the present wetting - drying algorithm, our results are compared with those achieved by previous studies. These results show the consistency with previous works done by [34] on water balance analysis, conducted for a period of 1997 - 2005 (Table 4). The differences can be explained by three reasons: (1) The study by [34] and ours were conducted for two different periods; (2) the results from [34] were based on a water balance model, considering overland flow, precipitation and evaporation, while SLIM results focused on surface water dynamics; and (3) the rating curves of the Tonle Sap characteristics were based on measured data in 2002 [49].

The hydraulic simulation conducted by [50] shows a maximum water volume of 77.5 km^3. The maximum discharges inward and outward the lake are 7900 m^3/s and 8200 m^3/s, respectively. These differences between the two results can be attributed to the fact that [50] performed their simulations based on data from 2002, that is a particular year with high flooding and two peaks in the whole Mekong basin. Moreover, the data used by [50] were not affected by the operation of the hydropower cascade in China that began in 2008 [35].

In [51], it is also stated that the maximum inflow and outflow discharge from the Mekong river to the lake observed in period of 2008 - 2010 were 7032 m^3/s and 8176 m^3/s. These values are approximated by the SLIM results as well.

Recently, [35] utilized remote sensing MODIS (Moderate Resolution Imaging Spectroradiometer) data from 2000 - 2014 to assess the variations of the Tonle Sap area. The minimum area is 2445 km^2, appearing in 2005 and the maximum area is 16508 km^2, appearing in 2011. The maximum values are approximately 20 % higher than our simulated results. This difference can be acceptable because inflows to the lake originate not only from the Mekong mainstream and tributaries but also from overland flow, precipitation and groundwater recharge in both wet and dry seasons [52].
The biggest differences between the SLIM results and other previous studies are the minimum values of water level, water area and water volume. However considering the measured data (see Fig. 13), the minimum water level observed in this period is 0.87 m, approximately 8 % lower than SLIM results, different values of the water area and water volume can be found in other works.

Table 4 Comparison with previous studies

Parameter	Water balance [34]	Hydro dynamics [50]	Measured data [48]	Satelite images [35]	SLIM results
Min water level (m)	1.19	-	-	-	0.95
Max water level (m)	10.36	-	-	-	9.98
Min surface area (km^2)	2061	-	-	2445	1200
Max surface area (km^2)	15280	-	-	16508	13329
Min water volume (km^3)	1.3	-	-	-	0.223
Max water volume (km^3)	76.1	77.5	-	-	69.9
Max inflow discharge (m^3/s)	-	7900	7032	-	7662
Max outflow discharge (m^3/s)	-	8200	8176	-	8160

3.4.5 The role of Tonle Sap system in the Mekong basin

During flooding phases, the water volume of Tonle Sap lake increases by about 69,560 km^3, from 0.356 km^3 to 69,916 km^3. A large amount of water from the Mekong river comes into the Tonle Sap lake. It means that the Lake works as a floodwater storage for the Mekong system, in particular for the Mekong Delta. During the dry season, a high discharge from the Tonle Sap lake flows to the Mekong Delta. It can reach to 5000 m^3/s, same as the one measured in Phnom Phenh. It confirms that the Tonle Sap lake is a major source of water for the Mekong Delta in the dry season.

3.4.6 Influence of the wetting - drying algorithm parameters on the model performance

To assess the influences of each the wetting - drying algorithm parameters (ε_1, ε_2 and ε_3) in the Mekong and the Tonle Sap simulation, we carrired out of a sensitivity analysis, some of the results of which are displayed in Fig. 20.
It is clear that the model can work well with $\varepsilon_1 \geq 0.1$ m, but not with $\varepsilon_1 = 0.01$ m, while the ε_2 was kept constant with value of 2 m and the value of ε_3 varied from

0.05 - 0.5 m (S2 and S3); and in case of $\varepsilon_1 = 0.05$ m, $\varepsilon_2 = 1$ m, $\varepsilon_3 = 0.25$ m (S4). This supports some of the results of section 2.4.1. and Fig. 4 that the model can only work with a ratio of the threshold thickness versus depth exceeding 0.2 %. If the ratio is less than 0.2 %, the model will stop because the non-linear Newton - Raphson solver does not converge. Specifically, in the runs S2 and S3, we keep the ε_1 value of 0.01 m and the ε_2 value of 2 m, the model stops at the iteration no. 76320 and 179712 (corresponding with 21 January 2009 - S2 and 14 January 2010 - S3 and see Fig. 20), respectively. The longer duration simulation is consistent with the larger ε_3 value of 0.5 m. By contrast, in the run S5, the threshold depth is increased to 0.25 m, the computation costs 9.5 days for simulating a hydrological year, that is approximately 2 times faster than the run S1 with the threshold depth of 0.1 m. However, to meet the requirement of mass conservation, we keep the thin layer thickness of 0.1 m for the Tonle Sap.

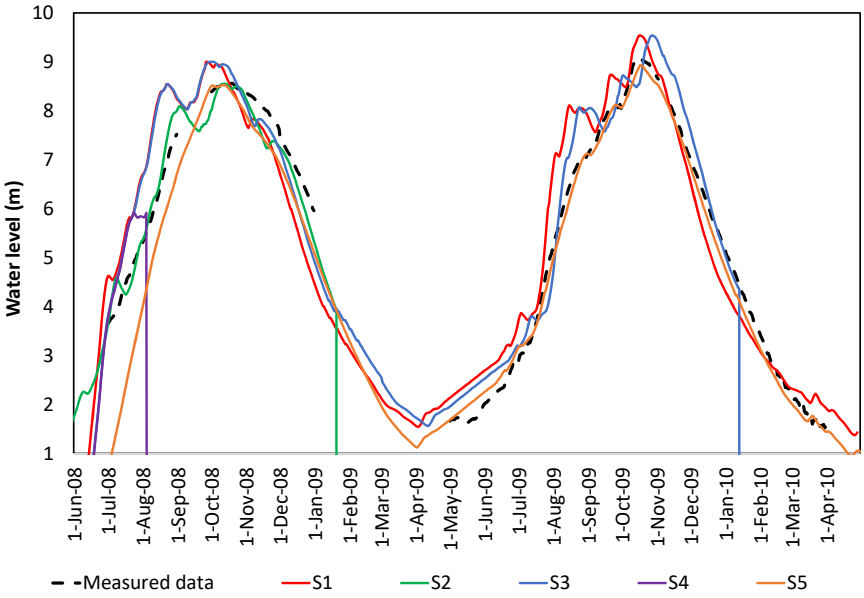

Fig. 20 Simulation of different wetting - drying parameters in two hydrological years 2008 and 2009. The black dash line presents for measured data, the red line (S1) shows the simulated results with $\varepsilon_1 = 0.1$ m, $\varepsilon_2 = 2$ m, $\varepsilon_3 = 0.5$ m, the green line (S2) shows the simulated results with $\varepsilon_1 = 0.01$ m, $\varepsilon_2 = 2$ m, $\varepsilon_3 = 0.05$ m, the blue line (S3) shows the simulated results with $\varepsilon_1 = 0.01$ m, $\varepsilon_2 = 2$ m, $\varepsilon_3 = 0.5$ m, the violet line (S4) shows the simulated results with $\varepsilon_1 = 0.05$ m, $\varepsilon_2 = 1$ m, $\varepsilon_3 = 0.25$ m, the orange line (S5) shows the simulated results with $\varepsilon_1 = 0.25$ m, $\varepsilon_2 = 5$ m, $\varepsilon_3 = 1$ m

4 Conclusions

The wetting - drying algorithm successfully implemented in SLIM reproduces well watering and dewatering processes in both theoretical test cases and in a realistic

domain. The method is based on a threshold value and a blending parameter. At each time step, the total water depth in each cell is compared to a user-defined threshold value. If the total water depth is lower than that value then that cell is considered dry. It shows both local mass conservation and rapid transition of a wet/dry interface.

The simulation results confirm that wetting - drying processes play an essential role in simulating the flow regime and water depth fluctuations of the Tonle Sap lake as well as the whole system. The simulation results also reveal the spatial and temporal distribution of the surface water areas and currents in the floodplain, which are controlled by imposed discharge from 12 tributaries as well as the water level in the downstream boundary at Phnom Phenh. Seasonal variations in the inundated area of the Tonle Sap lake are dominantly influenced by the flow regime in the Mekong River. The modelled results can also provide discharge and water level data at locations lacking monitoring of hydrological data. The model is confirmed to be a powerful tool to understand the flow dynamics of the Tonle Sap system as well as its hydrological roles in the Mekong Delta in both wet and dry seasons.

For future works, we do hope to improve our wetting - drying algorithm by converting parameters of wetting - drying algorithm (ε_1, ε_2, ε_3) to dimensionless parameters that would be valid for a large range of applications. With the improvement of the algorithm, we wish to conduct a further study on an extent domain including the Tonle Sap, the Cambodia floodplain and the Vietnam Mekong Delta to understand the watering and dewatering processes under various drivers. We should also take into account sediment and pollutant transport. As mentioned above, the interaction between surface water and groundwater is also an important component in the hydrological cycle. This is important because of increasing demands of freshwater for domestic uses and agricultural production.

Acknowledgements The PhD fellowship of Hoang-Anh Le is provided by the Université catholique de Louvain, Belgium. This research has been conducted under the framework of CARE - Rescif, Vietnam's initiative with grant number Tc-TTC-2017-08. Computational resources have been provided by the Consortium des Équipements de Calcul Intensif (CÉCI), funded by the Fonds de la Recherche Scientifique de Belgique (F.R.S.-FNRS) under Grant No.2.5020.11. E. Deleersnijder and S. Soares-Frazão are honorary research associates with F.R.S.-FNRS.

References

1. Burt TP (1996) The hydrological role of floodplains within the drainage basin system. In: Haycock NE, Burt TP, Goulding KWT, Piney G (ed) Buffer zones: their processes and potential in water protection, Haycock Associated Limited, UK, pp 21-32
2. Craig JF, Halls AS, Barr JJF, Bean CW (2004) The Bangladesh floodplain fisheries. Fisheries Research 66(2-3):271-286
3. Ward JV, Tockner K, Schiemer F (1999) Biodiversity of floodplain river ecosystems: ecotones and connectivity. River Research and Applications 15(13):125-139
4. Wheater H, Evans E (2009) Land use, water management and future flood risk. Land Use Policy 26:251-264
5. Baldwin DS, Mitchell AM (2000) The effects of drying and reflooding on the sediment and soil nutrient dynamics of lowland riverfloodplain systems: a synthesis. Regulated Rivers: Research & Management 16(5):457-467
6. Warner JC, Defne Z, Haas K, Arango HG (2013) A wetting and drying scheme for ROMS. Computers & Geosciences 58:54-61

7. Vater S, Beisiegel N, Behrens J (2015) A limiter-based well-balanced discontinuous Galerkin method for shallow-water flows with wetting and drying: One-dimensional case. Advances in Water Resources 85:1-13
8. Medeiros SC, Hagen SC (2013) Review of wetting and drying algorithms for numerical tidal flow models. International Journal for Numerical Methods in Fluids 71(4):473-487
9. DAlpaos L, Defina A (2007) Mathematical modeling of tidal hydrodynamics in shallow lagoons: A review of open issues and applications to the Venice lagoon. Computers & Geosciences 33(4):476-496
10. Kärnä T, De Brye B, Gourgue O, Lambrechts J, Comblen R, Legat V, Deleersnijder E (2011) A fully implicit wetting - drying method for DG-FEM shallow water models, with an application to the Scheldt Estuary. Computer Methods in Applied Mechanics and Engineering 200(5-8):509-524
11. Gourgue O, Comblen R, Lambrechts J, Kärnä T, Legat V, Deleersnijder E (2009) A flux-limiting wetting - drying method for finite-element shallow-water models, with application to the Scheldt Estuary. Advances in Water Resources 32(12):1726-1739
12. Dresback KM, Kolar RL, Dietrich JC (2002) Impact of the form of the momentum equation on shallow water models based on the generalized wave continuity equation. Development in Water Science 47:1573-1580
13. Casulli V (2009) A high resolution wetting and drying algorithm for free - surface hydrodynamics. International Journal for Numerical Methods in Fluids 60(4):391-408
14. Bradford SF, Sanders BF (2002) Finite-volume model for shallow-water flooding of arbitrary topography. Journal of Hydraulic Engineering 128(3):289-298
15. Begnudelli L, Sanders BF (2006) Unstructured grid finite-volume algorithm for shallow-water flow and scalar transport with wetting and drying. Journal of Hydraulic engineering132(4):371-384
16. Martins R, Leandro J, Djordjevic S (2018) Wetting and drying numerical treatments for the Roe Riemann scheme. Journal of Hydraulic Research 56(2):256-267
17. Heniche M, Secretan Y, Boudreau P, Leclerc M (2000) A two-dimensional finite element drying-wetting shallow water model for rivers and estuaries. Advances in Water Resources 23(4):359-372
18. Casulli, V., and Stelling, G. S. (1998). Numerical simulation of 3D quasi-hydrostatic, free-surface flows. Journal of Hydraulic Engineering 124(7), 678-686.
19. Candy, A. S. (2017). An implicit wetting and drying approach for non-hydrostatic baroclinic flows in high aspect ratio domains. Advances in Water Resources, 102, 188-205.
20. Chau, K. W. and Jiang, Y. W. (2002). Three-dimensional pollutant transport model for the Pearl River Estuary. Water Research, 36(8), 2029-2039.
21. Gourgue O, Deleersnijder E, White L (2007) Toward a generic method for studying water renewal, with application to the epilimnion of Lake Tanganyika. Estuarine, Coastal and Shelf Science 74(4):628-640
22. Lambrechts J, Humphrey C, McKinna L, Gourge O, Fabricius KE, Mehta AJ, Lewis S, Wolanski E (2010) Importance of wave-induced bed liquefaction in the fine sediment budget of Cleveland Bay, Great Barrier Reef. Estuarine, Coastal and Shelf Science 89(2):154-162
23. Gourgue O, Baeyens W, Chen MS, de Brauwere A, de Brye B, Deleersnijder E, Elskens M, Legat V (2013) A depth-averaged two-dimensional sediment transport model for environmental studies in the Scheldt Estuary and tidal river network. Journal of Marine Systems 128:27-39
24. De Brye B, Schellen S, Sassi M, Vermeulen B, Kärnä T, Deleersnijder E, Hoitink T (2011) Preliminary results of a finite-element, multi-scale model of the Mahakam Delta (Indonesia). Ocean Dynamics 61(8):1107-1120
25. Pham Van C, de Brye B, Deleersnijder E, Hoitink AJF, Sassi M, Spinewine B, Hidayat H, Soares-Frazo S (2016) Simulations of the flow in the Mahakam riverlakedelta system, Indonesia. Environmental Fluid Mechanics 16(3):603-633
26. Vallaeys V, Karna T, Delandmeter P, Lambrechts J, Baptista AM, Deleersnijder E, and Hanert E (2018) Discontinuous Galerkin modeling of the Columbia Rivers coupled estuary-plume dynamics. Ocean Modelling 124:111-124
27. Vincent D, Karatekin O, Vallaeys V, Hayes AG, Mastrogiuseppe M, Notarnicola C, Dehant V, Deleersnijder E (2016) Numerical study of tides in Ontario Lacus, a hydrocarbon lake on the surface of the Saturnian moon Titan. Ocean Dynamics 66(4):461-482
28. Smagorinsky, J. (1963). General circulation experiments with the primitive equations: I. The basic experiment. Monthly weather review, 91(3), 99-164

29. Balzano A (1998) Evaluation of methods for numerical simulation of wetting and drying in shallow water flow models. Coastal Engineering 34(1-2):83-107
30. Yuan D, Lin B, Falconer R (2008) Simulating moving boundary using a linked groundwater and surface water flow model. Journal of Hydrology 349(3-4):524-535
31. Nielsen C, Apelt C (2003) Parameters affecting the performance of wetting and drying in a two-dimensional finite element long wave hydrodynamic model. Journal of Hydraulic Engineering129(8):628-636
32. Kesserwani G, Liang Q (2012) Dynamically adaptive grid based discontinuous Galerkin shallow water model. Advances in Water Resources 37:23-39
33. Thacker WC (1981) Some exact solutions to the nonlinear shallow-water wave equations. Journal of Fluid Mechanics 107:499-508
34. Kummu M, Tes S, Yin S, Adamson P, Jozsa J, Koponen J, Richey J, Sarkkula J (2014) Water balance analysis for the Tonle Sap Lakefloodplain system. Hydrological Processes 28(4):1722-1733
35. Ji X, Li Y, Luo X, He D (2018) Changes in the Lake Area of Tonle Sap: Possible Linkage to Runoff Alterations in the Lancang River?. Remote Sensing10(6):866-886
36. Campbell IC, Say S, Beardall J (2009) Tonle Sap Lake, the heart of the lower Mekong. In: Campbell IC (ed) The Mekong, 1st ed, Academic Press, New York, pp 251-272
37. Siev S, Paringit EC, Yoshimura C, Hul S (2016) Seasonal Changes in the Inundation Area and Water Volume of the Tonle Sap River and Its Floodplain. Hydrology 3(4):33-45
38. Penny D (2006) The Holocene history and development of the Tonle Sap, Cambodia. Quaternary Science Reviews 25(3-4):310-322
39. Berg M, Stengel C, Trang PTK, Viet PH, Sampson ML, Leng M, Samreth S, Fredericks D (2007) Magnitude of arsenic pollution in the Mekong and Red River Deltas - Cambodia and Vietnam. Science of The Total Environment 372(2-3):413-425
40. Thanh VQ, Reyns J, Wackerman C, Eidam EF, Roelvink D (2017) Modelling suspended sediment dynamics on the subaqueous delta of the Mekong River. Continental Shelf Research 147:213-230
41. Royal Haskoning, Deltares, UNESCO - IHE (2010) The Flood Management and Mitigation Programme, Component 2: Structural Measures and Flood Proofing in the Lower Mekong Basin, Final Report, Volume 6C Integrated Flood Risk Management Plan for the West Bassac area in Cambodia. Mekong River Comission, Phnom Phenh
42. Hai PT, Masumoto T, Shimizu K (2008) Development of a twodimensional finite element model for inundation processes in the Tonle Sap and its environs. Hydrological Processes 22(9):1329-1336
43. Chau, K. W., and Jiang, Y. W. (2004). A three-dimensional pollutant transport model in orthogonal curvilinear and sigma coordinate system for Pearl river estuary. International Journal of Environment and Pollution.
44. Remacle JF and Lambrechts J (2018) Fast and robust mesh generation on the sphere - Application to coastal domains. Computer-Aided Design 103:14-23
45. Manh NV, Dung NV, Hung NN, Merz B, Apel H (2014) Large-scale suspended sediment transport and sediment deposition in the Mekong Delta. Hydrology and Earth System Sciences 18(8):3033-3054
46. Mekong River Commission (2015) Annual Mekong Flood Report 2011, Mekong River Commission, Phnom Phenh
47. Kummu M, Sarkkula J (2008) Impact of the Mekong River flow alteration on the Tonle Sap flood pulse. AMBIO 37(3):185-192
48. Asian Development Bank (2009) Cambodia: Preparing the Water Resources Management (Sector) Project. Water Resources Management Sector Development Project Technical Annex on Integrated Water Resources Management (IWRM). Ministry of Water Resources and Meteorology, Royal Government of Cambodia and Asian Development Bank, Phnom Penh
49. WUP-JICA (2004) Vol. II: Supporting Report, Paper IV: Development of Hydro-Hydraulic Model for the Cambodian Floodplains. Final report. JICA, Japan
50. Fujii H, Garsdal H, Ward P, Ishii M, Morishita K, Boivin T (2003) Hydrological roles of the Cambodian floodplain of the Mekong River. International Journal of River Basin Management 1(3):253-266
51. Lu X, Kummu M, Oeurng C (2014) Reappraisal of sediment dynamics in the Lower Mekong River, Cambodia. Earth Surface Processes and Landforms 39(14):1855-1865
52. May R, Jinno K, Tsutsumi A (2011) Influence of flooding on groundwater flow in central Cambodia. Environmental Earth Sciences 63(1):151-161